

Chemotaxis migration and morphogenesis of living colonies*

Martine Ben Amar^{1,2,a}

¹ Laboratoire de Physique Statistique, Ecole Normale Supérieure, UPMC Univ Paris 6, Université Paris Diderot, CNRS, 24 rue Lhomond, 75005 Paris, France

² Institut Universitaire de Cancérologie, Faculté de Médecine, Université Pierre et Marie Curie-Paris 6, 91 Bd de l'Hôpital, 75013 Paris, France

Received 19 December 2012 and Received in final form 27 March 2013

Published online: 27 June 2013

© The Author(s) 2013. This article is published with open access at Springerlink.com

Abstract. Development of forms in living organisms is complex and fascinating. Morphogenetic theories that investigate these shapes range from discrete to continuous models, from the variational elasticity to time-dependent fluid approach. Here a mixture model is chosen to describe the mass transport in a morphogenetic gradient: it gives a mathematical description of a mixture involving several constituents in mechanical interactions. This model, which is highly flexible can incorporate many biological processes but also complex interactions between cells as well as between cells and their environment. We use this model to derive a free-boundary problem easier to handle analytically. We solve it in the simplest geometry: an infinite linear front advancing with a constant velocity. In all the cases investigated here as the 3D diffusion, the increase of mitotic activity at the border, nonlinear laws for the uptake of morphogens or for the mobility coefficient, a planar front exists above a critical threshold for the mobility coefficient but it becomes unstable just above the threshold at long wavelengths due to the existence of a Goldstone mode. This explains why sparsely bacteria exhibit dendritic patterns experimentally in opposition to other colonies such as biofilms and epithelia which are more compact. In the most unstable situation, where all the laws: diffusion, chemotaxis driving and chemoattractant uptake are linear, we show also that the system can recover a dynamic stability. A second threshold for the mobility exists which has a lower value as the ratio between diffusion coefficients decreases. Within the framework of this model where the biomass is treated mainly as a viscous and diffusive fluid, we show that the multiplicity of independent parameters in real biologic experimental set-up may explain varieties of observed patterns.

1 Introduction

Chemotaxis plays an important role in many biological processes like wound healing, cancer metastasis and fertilization. In colonies or tissues, chemotaxis leads to collective motions regulated by biological processes like cell-cell interactions, adhesion to the substrate, secretion of growth factor or inhibitors. At the origin of this process morphogens are long-range molecules that induce concentration cellular responses, activating different transcriptional pathways [1]. In embryogenesis, diffusion of these species is at the origin of the “French flag model” where cell fates are simply explained by their concentration gradients. Here, we aim to investigate the role of these chemoattractants in two-dimensional migration of bacteria or cells in an epithelium. Our scope is to give a unified picture of these two

different experimental *in vitro* situations and to present a continuous formalism of the shape of the colony during migration.

Morphogens diffuse while up-taken at the surface of the cells by complex chemo-receptors [2]. Chemotactic pathways for bacteria allow motile bacteria to navigate according to higher concentration of attractants. Colonies exhibit various patterns going from rather compact and cohesive to dendritic (even fractal in extreme cases) structures. In a pioneering review [3] Ben Jacob and collaborators have underlined the close similarity between bacteria colonies (in a Hele-Shaw cell) and patterns in physics experiments like dendritic crystallization [4–6], viscous fingering [7,8] and electro-chemical deposition [9,10]. However, the bacterial pattern differs depending on the species, the nutrient conditions and also the substrate, exhibiting diverse morphologies including Eden-like growth, fractal and dense branching morphologies (see the review by Ben-Jacob and Levine [11]). Epithelia are more compact, cells spread as a thin layer over a flat surface in a Petri dish. Fronts are

* Contribution to the Topical Issue “Physical constraints of morphogenesis and evolution”, edited by Vincent Fleury, Paul François and Marie Christine Ho Ba Tho.

^a e-mail: benamar@lps.ens.fr

denser compared to bacteria [12] even if some fingering instabilities may also appear.

All these patterns are reminiscent of diffusive instabilities but the relation between solidification or viscous fingering experiments is not obvious *a priori*. Here we present a continuous model of chemotaxis migration in the framework of the mixture models [13,14] with two phase constituents. In principle, this model can incorporate an arbitrary number of constituents described by a density and a velocity field defined on an intermediate scale between the constituent and the experimental set-up size. In this work, one phase is water while the other phase is a mixing of water and cells: bacteria or epithelium cells. We assume the horizontal size of the Petri dish or the Hele-Shaw cell infinite as the domain of the colony and we examine the evolution of this colony under a chemotactic gradient. We limit ourselves to the case of chemoattractants (the cells swim up gradients of morphogens), not the case of chemorepellants [15]. The mixture model is suitable for numerical investigations but here we use it to transform the front dynamics into a free-boundary problem. The boundary of the colony evolves according to a diffusion equation with an uptake term while at the unknown border boundary conditions are applied. Indeed when the transition zone is sharp enough, it appears as a zone of discontinuities between two domains. Boundary conditions depend on the biological processes involved in the model such as an increase of mitosis at the front as observed in recent experiments [16].

The derived sharp interface model is then a free-boundary problem as in dendritic growth or viscous fingering formulation. It has the advantage to be simple enough to allow analytical treatments for the existence and stability of fronts. It can appear as a new variant of the Keller-Segel [17] model of chemotaxis, originally written to explain aggregation of amoebae and which has been widely studied in mathematical biology. It is known to generate finite time singularities showing its intrinsic instability [18–20]. Once transformed into a free-boundary problem, our model indicates that planar fronts remain unstable for chemoattractants due to the existence of a Goldstone mode and a behavior in k^2 for the growth rate of weak perturbations at long wavelengths. This is mainly true for weak chemotaxis and hence, weak velocities. Although capillary effects stabilize the front at short wavelengths, it is not enough to circumvent the intrinsic instability of the Keller-Segel [17] model. However when chemotaxis increases above a critical threshold for the mobility coefficient, surprisingly the front recovers the stability. We examine also other physical effects present in practice in experiments like the diffusion in 3 dimensions or nonlinearities which have been extensively introduced in mathematical biology.

Nonlinearities occurring in the chemoattractant diffusion itself, the uptake or the mobility law introduce complexity in the analytical predictions and we consider only the last two cases. For the uptake process of the chemoattractants by the cells, the Michaelis Menten [21] law is very commonly used in bacteria simulations [22]. This nonlinearity does not suppress the Goldstone mode but may

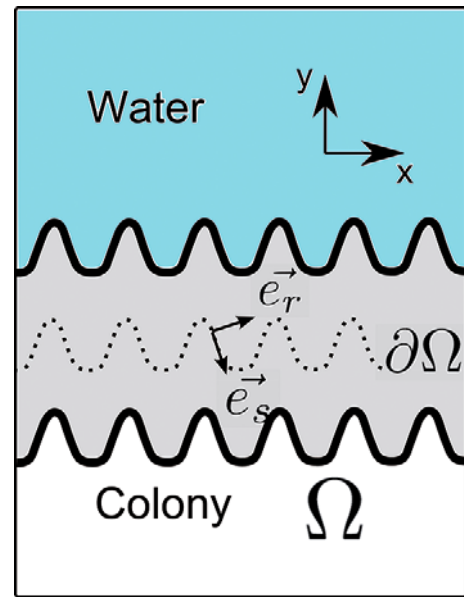


Fig. 1. Schematic representation of a top view of the Hele-Shaw cell containing the colony in the domain Ω . The interface $\delta\Omega$ is wavy and is assumed to have a small extension compared to the Hele-Shaw cell size.

change the behavior at long wavelengths. Surprisingly a much more stabilizing effect is induced by a nonlinearity in the chemotactic mobility as a function of the chemoattractant concentration. In this case we demonstrate that planar traveling-wave stable solutions exist. The mixture model can be extended to incorporate short-range or elastic interactions like it has been done for tumor growth with adhesion to a soft substrate [23]. Our work will open new possibilities for growth of epithelia once introduced more solid interactions in the growth process. It might be a way to explain the relative stability of epithelium growth *in vitro* [24,25].

The paper is organized as follows: Section 2 presents the continuous model for chemotaxis, including diffusion, interaction between cells, the morphogen uptake and mitosis. Section 3 gives the asymptotic analysis allowing the transformation of coupled partial differential equations into a free-boundary problem which is easier for analysis. Section 4 gives the results of the model: the existence of traveling wave solutions, the stability of these solutions according to a restricted number of dimensionless parameters. The end of sect. 4 concentrates on the possibility of suppressing the Goldstone mode by introducing various realistic effects like mitosis at the border and nonlinearities. Section 5 compares the results to experiments. Finally in conclusion we sum up the main theoretical results.

2 The continuous model for chemotaxis

We consider a two-dimensional cell population of density ρ_s immersed in a morphogenetic gradient. This population can be bacteria in a Hele-Shaw cell, bacteria in a thin film put on a solid substrate or an epithelium grow-

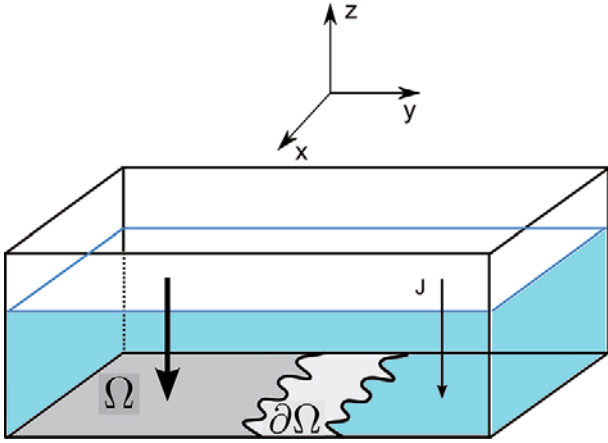


Fig. 2. Schematic representation of a Petri dish containing a growing epithelium in the domain Ω . The interface $\delta\Omega$ is wavy and is assumed to have a small extension. A flux with a decreasing intensity from left to right is indicated to show the diffusion in the vertical direction.

ing on a substrate. Initially located in a domain Ω , with a front separation $\delta\Omega$ (see figs. 1 and 2), the colony moves in the direction of the highest chemoattractant concentration. When they are also nutrients, the colony also grows by cell division. Both processes are considered but we will focus mostly on migration.

2.1 Description of the cellular population

We adopt here a continuous model for the cells immersed in a liquid bath (see figs. 1 and 2). For growing epithelia on a substrate, like in wound healing mimetic experiments [25], the fact that the tissue remains a monolayer ensures the 2D characteristic of the migration even if the experiment takes place in a 3D Petri dish. For bacteria, on the contrary, the 2D hallmark is obtained by confinement in a Hele-Shaw cell or when bacteria grow making a thin film. We will not consider this last possibility here although adaptation of our model can be done for biofilms. In both cases (epithelia or bacteria), the colony is assumed to live in a flat land saturated by nutrients. We assume that the cellular population is located in an infinite domain Ω represented by $y < 0$ in Cartesian coordinates. Our sample being a mixture of two species with the same mass density, the density of water, we call ρ_l and ρ_s the concentration in each phase with $\rho_l + \rho_s = 1$. Far away from $\delta\Omega$, for y positive $\rho_l = 1$ and $\rho_s = 0$. For $y \rightarrow -\infty$ ρ_l and ρ_s reach constant values: $\rho_s = \rho_\infty$ and $\rho_l = 1 - \rho_\infty$. For epithelia only, when the tissue is at confluence, $\rho_s = \rho_\infty = 1$ and the layer thickness h_0 is then constant. At the front it decreases and this variation [16] can be taken into account in our model by an increase of ρ_l . Each phase has locally a velocity (\mathbf{v}_l or \mathbf{v}_s) and the average velocity is then given by $\mathbf{V} = \rho_l \mathbf{v}_l + \rho_s \mathbf{v}_s$. We consider now the diffusion of the nutrients with concentration \tilde{c} .

2.2 Morphogen diffusion in a Hele-Shaw cell and definition of the physical units

We begin by the bacteria (Hele-Shaw cell). The nutrients may play different roles and we will try to involve all of them in the same formalism. Being chemoattractants, they are the motor of the migration but they will be absorbed by the cells for proliferation or simply because of surface adhesion. Choosing the uptake time τ_c as time unit and calling D_l the morphogen diffusion coefficient in the liquid phase, we define a length scale by l_0 such that $l_0^2 = D_l \tau_c / \rho_\infty$ and a velocity unit given by $l_0 / \tau_c = \sqrt{D_l / (\rho_\infty \tau_c)}$. The validity of the model requires l_0 to be much bigger than the cell size. *All the equations presented hereafter are dimensionless.* The chemoattractant concentration $c = \tilde{c} / c_\infty$ satisfies a 2D diffusion equation given by

$$\partial_t c + \mathbf{V} \cdot \nabla c = \nabla D(\rho_s) \nabla c - c \rho_s, \quad (1)$$

∇ being the horizontal dimensionless gradient $\nabla = (\partial_x, \partial_y)$ and $D(\rho_s) = (\beta - 1)(\rho_s / \rho_\infty) + 1$. Clearly the morphogens are consumed only if members of the colony exist, *i.e.* for nonvanishing ρ_s . c and ρ_s are space and time dependent. Let us examine now the epithelium migration in a Petri dish according to figs. 2 and 3.

2.3 Morphogen diffusion in a Petri dish

The same equation in 3D for nutrient diffusion in a Petri dish with a localized absorption at $z = 0$ shows an additive term and we get

$$\partial_t c_{3d} + \mathbf{V} \cdot \nabla c_{3d} = \nabla_2 D(\rho_s) \nabla_2 c_{3d} + \frac{\partial^2 c_{3d}}{\partial z^2} - c_{3d} \rho_s, \quad (2)$$

with $c_{3d} = c_{3d}(x, y, z, t)$ being now a function of all coordinates while ρ_s remains a function of the horizontal position only. In this case the saturation condition $\tilde{c}_{3d} = c_\infty = 1$ has to be applied for $z = H$, the position of the upper bath surface and we assume that H is a large quantity (much larger than our length unit and the thickness of the epithelium h_0). This hypothesis is checked in the experiment [25]. In this context, considering a distance d intermediate $h < d < H$, one can expand the density c as

$$c_{3d}(x, y, z, t) = c_0(x, y, t) + \epsilon_1^2 c_1(x, y, Z) + O(\epsilon_1^4), \quad (3)$$

with $\epsilon_1 = d/H$ and $Z = z/\epsilon_1$. To leading order, we get

$$\partial_t c_0 + \mathbf{V} \nabla c_0 = \nabla D(\rho_s) \nabla c_0 + \frac{\partial^2 c_1}{\partial Z^2} - c_0 \rho_s + O(\epsilon_1^2). \quad (4)$$

Above the distance d we assume that the saturation is provided by a continuous vertical flux, a valid assumption if H is much smaller than the lateral size of the Petri dish. This flux being amplified when the absorption process increases, we have $\partial_z c_{3d} = \alpha(1 - c_0)d$. Averaging the concentration gives

$$c(x, y, t) = \langle c_{3d} \rangle = \frac{1}{d} \int_0^d c_{3d}(x, y, z, t) dz, \quad (5)$$

then in the layer d eq. (4) is transformed into

$$\partial_t c + \mathbf{V} \nabla c = \nabla (\beta \rho_s + 1 - \rho_s) \nabla c - c(\rho_s + \alpha)/(1 + \alpha) + \alpha/(1 + \alpha), \quad (6)$$

where a correction of the length unit has been introduced to take into account the transverse flux in 3D: ($\tilde{l}_0 = l_0/\sqrt{1 + \alpha}$). The average concentration satisfies a 2D diffusion equation with an additive contribution due to the transverse flux. The depletion of the nutrients has to be decomposed into two contributions: one occurring at the border due to possible mitosis activity (not yet introduced in eq. (6)), the second present in eq. (6) acting on the scale of the colony. Both effects may have also different amplitudes. A more detailed description will be given hereafter. To solve one of these diffusion equations (1), (6) one needs to know the colony density ρ_s and the velocity \mathbf{V} . This is the aim of the next section.

2.4 Cellular density repartition and dynamics

We present here the mixture model mainly used in the context of tumor growth which constitutes a rather intuitive formalism when dynamics, growth, interactions between species and dissipation occur. We describe this model in the following and applied it to chemotaxis migration. This model [13,14] concerns a mixture of species in interaction which move according to mechanical laws. Being continuous it is valid for processes occurring at a scale larger than the size of the cells. For our purpose we limit ourselves to a two-phase model, mainly the cells and water, but the model can be extended easily to an arbitrary number of species. The species are then described by an average density ρ_i and average velocity \mathbf{v}_i , the average being made at an intermediate scale between the cellular and the experimental sizes. These quantities are then space and time dependent. When the mixture contains much smaller elements like morphogens or nutrients, they are not considered as part of the mixture. However, they will modify either the dynamics or the species repartition. We represent chemotaxis by a simple linear relation between the cell velocity and the gradient relative to the concentration at the origin of a forcing velocity: $\tilde{\mathbf{v}}_s = -\Lambda \nabla c$ in physical units, being simplified in $\mathbf{v}_s = -\Lambda \nabla c$ in dimensionless units with $\Lambda = \tilde{\Lambda} c_\infty \rho_\infty / D_l$. More complex choices with nonlinearities can be found in the abundant literature on the subject [18,19] and will be discussed in sect. 4. The mass balance equation written in dimensionless units reads

$$\partial_t \rho_s + \nabla \cdot \rho_s (\mathbf{v}_s - \Lambda \nabla c) = \gamma, \quad (7)$$

γ being the cell proliferation rate. For the liquid phase an equivalent equation with $\rho_l = 1 - \rho_s$ reads

$$\partial_t \rho_l + \nabla \cdot \rho_l \mathbf{v}_l = \gamma_l = -\gamma. \quad (8)$$

Since the mass density of cells and water is very similar, we have $\gamma_l = -\gamma$. The average velocity is given by

$$\mathbf{V} = \rho_s \mathbf{v}_s + \rho_l \mathbf{v}_l, \quad (9)$$

with the incompressibility condition transformed into

$$\nabla \cdot (\mathbf{V} - \rho_s \Lambda \nabla c) = 0. \quad (10)$$

We assume a free energy \mathcal{F}_s for representing the attraction between cells

$$\mathcal{F}_s = \int_{\mathcal{R}^2} dx dy (\Psi(\rho_s) + \epsilon^2 |\nabla \rho_s|^2), \quad (11)$$

where a penalty energy has been added for sharp density gradients. Dissipation in this system is due to the friction with the substrate or friction between phases. Assuming a viscous drag between phases, the variation of energy per unit times called \mathcal{Q} is then

$$\begin{aligned} \mathcal{Q} = \int_{\mathcal{R}^2} & \left[\underbrace{\frac{M \rho_s \rho_l}{2} (\mathbf{v}_s - \mathbf{v}_l)^2 + \frac{M_s \rho_s^2}{2} \mathbf{v}_s^2 + \frac{M_l \rho_l^2}{2} \mathbf{v}_l^2}_{\text{dissipation}} \right. \\ & + \underbrace{\left(\frac{\partial \Psi}{\partial \rho_s} - \epsilon^2 \Delta \rho_s \right) (-\nabla \cdot (\rho_s (\mathbf{v}_s - \Lambda \nabla c) + \gamma))}_{\text{variation of free energy}} \\ & \left. - \underbrace{p \nabla \cdot (\rho_s \mathbf{v}_s + \rho_l \mathbf{v}_l - \rho_s \Lambda \nabla c)}_{\text{incompressibility}} \right] dx dy. \quad (12) \end{aligned}$$

The pressure p ensures the incompressibility of the mixture, the coefficient M refers to the friction between both phases, M_l and M_s represent either the fluid friction with a stiff static substrate or the internal viscous dissipation. \mathcal{Q} has been called Rayleighian in [26] and appears as the equivalent of the Lagrangian for dissipative systems. As a consequence, our formalism is purely mechanical and does not introduce any thermodynamic concept as phase-field models for example [27,28]. The first term of eq. (12) exists only if both phases exist at an arbitrary point which explains the factor ρ_l and ρ_s , the same argument being applied to the second and third term of eq. (12). This energy rate \mathcal{Q} must be an extremum which gives by elementary variation analysis with respect to both velocities ($\mathbf{v}_s, \mathbf{v}_l$)

$$\mathbf{v}_s = -\mathcal{A} \cdot \nabla p - \mathcal{B} \cdot \nabla \left(\frac{\partial \Psi}{\partial \rho_s} - \epsilon^2 \Delta \rho_s \right), \quad (13)$$

$$\mathbf{V} = \rho_s \mathbf{v}_s + \rho_l \mathbf{v}_l = -\mathcal{C} \cdot \nabla p - \mathcal{D} \cdot \nabla \left(\frac{\partial \Psi}{\partial \rho_s} - \epsilon^2 \Delta \rho_s \right), \quad (14)$$

with

$$\mathcal{A} = \frac{(M + M_l \rho_l)}{\mathcal{M}}, \quad \mathcal{B} = \frac{(M \rho_s + M_l \rho_l)}{\mathcal{M}},$$

with

$$\mathcal{C} = \frac{M + (M_l + M_s) \rho_l \rho_s}{\mathcal{M}}, \quad \mathcal{D} = \frac{(M + M_l \rho_l) \rho_s}{\mathcal{M}},$$

and

$$\mathcal{M} = M M_s \rho_s^2 + M_s M_l \rho_l \rho_s + M M_l \rho_l^2. \quad (15)$$

Introducing the incompressibility condition eq. (10) into eq. (14) allows to calculate the pressure p as usually done

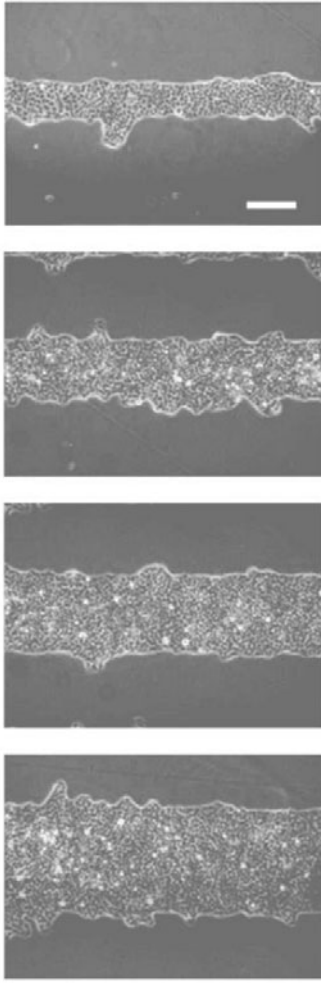


Fig. 3. A sequence of a growing epithelium stripe of MDCK cells according to the technique of stencil assay [25]. The bar means $200 \mu\text{m}$, the duration time is 8 hours. Courtesy of Pascal Silberzan.

in hydrodynamics. Once p is introduced into eq. (13) we deduce \mathbf{v}_s as a function of ρ_s and finally eq. (7) gives the density ρ_s for a given interaction potential $\Psi(\rho_s)$ and the growth rate γ .

At this stage, the presentation of the model is complete and ready for numerical simulations. It is an alternative to phase-field models [27,28]. Another possibility is to derive the asymptotic sharp interface limit and transform this set of coupled partial differential equations into a free-boundary problem. Free-boundary problems allow to predict analytically the front morphology in simple initial geometries: planar and circular fronts, while continuous models are more easy to implement in numerical front simulations.

3 Morphogenesis free-boundary problem

We consider now the asymptotic limit of our system of eqs. (1), (6), (14) far away from the interface. It corresponds also to the equations we have to solve in the sharp interface limit.

3.1 Bulk equation

In Ω , the cell density ρ_s has reached its constant value ρ_∞ . Cell divisions if they occur are localized at the interface border, and hence γ vanishes far away from this border and constant values are reached for ρ_l and ρ_s . Taking \mathbf{V} from eq. (14) gives

$$\mathbf{V} = -\mathcal{C}_\infty \nabla p, \quad (16)$$

where \mathcal{C}_∞ is the asymptotic limit of \mathcal{C} with $\rho_s = \rho_\infty$ and $\rho_l = 1 - \rho_\infty$. Note that for epithelia, \mathcal{C}_∞ is equal to $1/M_s$. Hereafter we will use capital quantities for the asymptotic values or for the sharp interface model. Equation (16) means simply a Darcy flow both for a dilute bacteria bath but also for tissues when the hydrostatic part dominates the shear stresses. Far away from the front but in water now, $\rho_s = 0$ and $\rho_l = 1$. We have also a Darcy law with a constant permeability M_l . Defining $P = \mathcal{C}_\infty \cdot p$ the hydrodynamic flow equation in Ω becomes

$$\mathbf{V}_s = -\nabla P, \quad \text{with} \quad \nabla^2(P + \Lambda c) = 0, \quad (17)$$

while in water it is

$$\mathbf{V}_l = -\frac{1}{(\mathcal{C}_\infty M_l)} \nabla P, \quad \text{with} \quad \nabla^2 P = 0. \quad (18)$$

When the ratio of permeability $\mathcal{C}_\infty M_l$ is weak we can neglect the flow in the liquid and have $P = 0$. For the concentration field, we need simply to consider eq. (1) or eq. (6) with $\rho_s = 0$ in the liquid and $\rho_s = \rho_\infty$ in the colony. We examine now the boundary conditions.

3.2 Boundary conditions

The correct boundary conditions to apply in the sharp interface limit come from the inner domain around $\partial\Omega$ when $\epsilon \rightarrow 0$. The asymptotic analysis is not difficult but a little technical. We give here the outline of the proof. First, as for phase-field models [27,28], we define a dimensionless order parameter ϕ which will vary between -1 and 1 across the tiny boundary layer, the interface itself being defined by $\phi = 0$. So we get

$$\rho_s = (1 - \phi)\rho_\infty/2 \quad (19)$$

and $\rho_l = 1 - \rho_s = (1 + \phi)\rho_\infty/2$. We define a local coordinate system on the line $\delta\Omega$ (see fig. 1), the unit vectors being the tangent and normal to this line. We solve eqs. (6), (14) in this frame of coordinates assuming the following scaling for ϕ , p and c as a function of $R = r/\epsilon$ and S

$$\begin{aligned} \phi(R, S) &= \phi_0(R, S) + \epsilon\phi_1(R, S) + O(\epsilon^2), \\ p(R, S) &= \epsilon p_0(R, S) + O(\epsilon^2), \\ c(R, S) &= C_0(r, S) + \epsilon c_0(R, S) + O(\epsilon^2). \end{aligned} \quad (20)$$

Here we make the assumption that the concentration field $c(R, S)$ is continuous at leading order and may present a sharp variation only at first order.

3.2.1 Pressure jump at the interface

A sharp transition zone is obtained for typical energy interactions with two wells such as in the Cahn-Hilliard model [29,30]: $\Psi = f_0(-\phi^2/2 + \phi^4/4)$. This choice has the advantage to give analytical results [31]. Combining eq. (10) with eq. (14), taking into account the scaling defined by eqs. (20), the leading contribution is then:

$$\mathcal{L}(\phi_0) = \frac{\partial^2 \phi_0}{\partial R^2} + a^{-2} \phi_0(1 - \phi_0^2) = 0 \quad \text{with} \quad a^2 = \frac{\rho_\infty^2}{4f_0}, \quad (21)$$

which gives

$$\phi_0(R) = \tanh\left(\frac{R}{a}\right). \quad (22)$$

The next order gives

$$\frac{2\Lambda_0 \rho_s}{\mathcal{D} \rho_\infty} \frac{\partial c_0}{\partial R} + \frac{2\mathcal{C}}{\mathcal{D} \rho_\infty} \frac{\partial p_0}{\partial R} - \kappa \frac{\partial^2 \phi_0}{\partial R^2} - \frac{\partial}{\partial R} \mathcal{L}_1(\phi_1) = 0, \quad (23)$$

with κ the local curvature, positive for the convex part of the interface and $\mathcal{L}_1(\phi_1)$ denotes

$$\mathcal{L}_1(\phi_1) = \frac{\partial^2 \phi_1}{\partial R^2} + a^{-2}(1 - 3\phi_0^2)\phi_1. \quad (24)$$

Equation (23) is an equation for ϕ_1 once p_0 and c_0 are known. However one needs to ensure convergence of the expansion given by eq. (20), so one needs that ϕ_1 and all its derivatives cancel at both $\pm\infty$. Since $\partial\phi_0/\partial R$ is a solution of $\mathcal{L}_1 = 0$, the theorem of the adjoint imposes

$$\frac{2}{\rho_\infty} \int_{-\infty}^{\infty} \left(\frac{\Lambda_0 \rho_s}{\mathcal{D}} \frac{\partial c_0}{\partial R} + \frac{\mathcal{C}}{\mathcal{D}} \frac{\partial p_0}{\partial R} \right) (1 - \phi_0) dR = \kappa \int_{-\infty}^{\infty} \left(\frac{\partial \phi_0}{\partial R} \right)^2 dR. \quad (25)$$

Noticing that the integrand of the left-hand side is well behaved at both infinities, we integrate by part to extract the main contribution of the left-hand-side and we derive:

$$\{p_0\} = \frac{1}{4} \rho_\infty \frac{\mathcal{D}_\infty}{\mathcal{C}_\infty} \kappa \int_{-\infty}^{\infty} \left(\frac{\partial \phi_0}{\partial R} \right)^2 dR - \frac{\Lambda}{\mathcal{C}_\infty} \{c_0\}, \quad (26)$$

where $\{p_0\}$ means the pressure jump between its value at the interface ($\phi = 0$) and its value at $R \rightarrow -\infty$ ($\phi = -1$), the same definition applies to $\{c_0\}$. We transform eq. (26) into

$$\{p_0\} = \frac{1}{\mathcal{C}_\infty} \frac{\sigma}{\epsilon} \kappa - \frac{\Lambda}{\mathcal{C}_\infty} \{c_0\}. \quad (27)$$

Equation (26) gives for our ‘‘mixture’’ the equivalent of a Laplace contribution with an additive correction when the concentration is discontinuous at the interface. Coming back to P we get the pressure jump as

$$\{P\} = \sigma \kappa - \Lambda \epsilon \{c_0\}, \quad (28)$$

which is the boundary condition for the pressure.

3.2.2 Conditions on the normal velocities at the moving front

The moving front is given by $\delta\Omega$ defined by $\phi = 0$. Examining eq. (7) written in the local moving frame of $\delta\Omega$, we get

$$\frac{\partial}{\partial R} \rho_s (v_s - \Lambda_0 \nabla c) = \epsilon \gamma = \frac{4ac}{\rho_\infty^2} \rho_s (\rho_\infty - \rho_s) \Gamma_1, \quad (29)$$

where γ scales as $1/\epsilon$ so has a noticeable amplitude at the front but cancels in the liquid and also when the tissue is at confluence $\rho_s \rightarrow \rho_\infty$. γ depends also on the availability of the nutrients. We make the simplest linear choice and assume that at the front $C_0(S)$ the concentration of nutrients depends only on the arc-length (smooth variation of the concentration field). Taking into account eq. (19), the right-hand side can be transformed into $a\Gamma_1(1 - \phi^2)C_0$. Integrating between the interface ($\phi = 0$) and $-\infty$ (with $\phi = -1$) we get the interfacial boundary condition for the cell velocities in the normal direction of the front

$$(\mathbf{V} - \mathbf{V}_{\delta\Omega}) \cdot \mathbf{N} = -\Gamma_1 C_0, \quad \text{so} \quad \mathbf{N} \cdot \mathbf{V}_{\delta\Omega} = -\mathbf{N} \cdot \nabla P + \Gamma_1 C_0, \quad (30)$$

where $V_{\delta\Omega} = \partial_t \delta\Omega$.

3.2.3 Boundary conditions for the chemoattractant concentration

Mitotic activity localized at the front induces a supplementary absorption of nutrients at this front. Our work hypothesis is that this additional depletion will not perturb too much the concentration field which will remain continuous even in the sharp interface limit. It means that the additive term we must add to eq. (1) or eq. (6) will have the same dependence as in eq. (29) but with a different constant Γ_2 . In the local coordinate frame both diffusion equations reduce to

$$\partial_t c + \frac{1}{\epsilon} V_R \partial_R c = \frac{1}{\epsilon^2} \partial_R D(\phi) \partial_R c - \frac{a}{2\epsilon} \Gamma_2 c (1 - \phi^2), \quad (31)$$

with

$$D(\phi) = (\beta - 1) \rho_s / \rho_\infty + 1 = \frac{1}{2} [\beta + 1 + (1 - \beta) \phi_0(R)].$$

Expanding the concentration field according to eq. (20), we get that the main order is a slowly varying function of the orthogonal coordinate r : $C_0(r, S)$. Next order in ϵ gives

$$\partial_R D(\phi) \partial_R c_1 - (a/2) \Gamma_2 C_0 (1 - \phi^2) = 0, \quad (32)$$

which gives for $R \rightarrow -\infty$ (or $r \rightarrow 0^-$)

$$\beta \partial_R c_1 = \beta \partial_r C_0 = -(\Gamma_2/2) C_0 + f(S) \quad (33)$$

and for $R \rightarrow \infty$ (or $r \rightarrow 0^+$)

$$\partial_R c_1 = \partial_r C_0 = (\Gamma_2/2) C_0 + f(S), \quad (34)$$

where capital letters mean functions defined out of the boundary layer, $f(S)$ being an arbitrary function of the arc-length. So at zero order we get a continuous concentration field $C_0(r, S)$, with a discontinuity in the normal gradient, the discontinuity in the concentration appearing only at first order in ϵ . It will be discarded. Restricting to the zero order, we finally derive the boundary condition when a localized mitosis production occurs at the front

$$C_s(0) = C_l(0) = C_0 \text{ on } \partial\Omega \quad (35)$$

and

$$\beta \mathbf{N} \cdot \nabla C_s - \mathbf{N} \cdot \nabla C_l = -\Gamma_2 C_0 \text{ on } \partial\Omega. \quad (36)$$

Finally we present a summary of the set of equations which constitutes the sharp-interface limit.

3.2.4 Summary for the sharp-interface model

We take the convention to use capital letters for physical quantities in the sharp-interface limit. We detail now these equations in the liquid and in the colony phase. Neglecting the fluid convection, the diffusion equation in the liquid is given by

$$\partial_t C_l = \nabla^2 C_l - \delta(C_l - 1), \quad (37)$$

with $\delta = \alpha/(\rho_\infty + \alpha)$. In the colony we have

$$\partial_t C_s = \beta \nabla^2 C_s - C_s + \delta. \quad (38)$$

Boundary conditions to apply at $\delta\Omega$ is the continuity of C and the discontinuity of the normal gradient $\mathbf{N} \cdot \nabla C$

$$\begin{aligned} C_l &= C_s \text{ and } \mathbf{N} \cdot \nabla C_l = \beta \mathbf{N} \cdot \nabla C_s + \Gamma_2 C_s \text{ on } \delta\Omega, \\ C_l &= 1 \text{ when } y \rightarrow \infty, \end{aligned} \quad (39)$$

with \mathbf{N} the normal to the interface. The front velocity is given by the displacement of the cells

$$\mathbf{V}_s = -\nabla P \text{ with } \nabla^2(P + \Lambda C) = 0. \quad (40)$$

We assume the viscosity of water negligible. Boundary conditions for hydrodynamics are then

$$\begin{aligned} \mathbf{N} \cdot \partial_t \Omega &= \mathbf{N} \cdot \mathbf{V}_s + \Gamma_1 C_s, \\ P &= \sigma \kappa. \end{aligned} \quad (41)$$

If we neglect mitosis, and focus on front migration, there exists 2 independent parameters which are Λ and σ in the 2D case, 3 in the 3D case with δ . The two first are related to physical and biological quantities that we recall here:

$$\Lambda = \tilde{\Lambda} \left(\frac{c_\infty \rho_\infty}{D_l} \right), \quad \text{while} \quad \sigma = \tilde{\sigma} \left(\frac{K \rho_\infty^3}{D_l^{3/2} \tau_c^{1/2}} \right), \quad (42)$$

α or δ are parameters much more difficult to evaluate. Indeed it is the result of viscous and chemical boundary layers. It changes the effective diffusion coefficient which becomes $D_l \rightarrow D_L/(1 + \alpha)$, decreasing the length and the velocity units. Let us study the role of these different dimensionless parameters for the existence of planar solutions.

4 Steady planar front

4.1 Conditions for the existence of steady fronts

Examining more carefully the set of equations, one notices that our growth problem couples a diffusion equation with consumption and a Laplace equation typical of viscous fingering. Being a more complex front dynamics than dendritic or viscous fingering front, we examine the existence of steady solutions moving along the y -axis at constant velocity U and we analyze their stability. In the moving frame, going towards the highest concentration of the chemical signal, the diffusion equation setting $C_\infty = 1$ for $y \rightarrow +\infty$, the continuity of C and the discontinuity of the chemical flux represented by eq. (39) at the free surface gives

$$C_0(Y) = \begin{cases} \delta + (C_0(0) - \delta)e^{r_s Y/(2\beta)}, & \text{for } Y = y - Ut \leq 0, \\ 1 + (C_0(0) - 1)e^{-r_l Y/2}, & \text{for } Y = y - Ut \geq 0, \end{cases} \quad (43)$$

with

$$\begin{aligned} C_0(0) &= (r_l + \delta r_s)/(2\Gamma_2 + r_l + r_s), \\ r_l &= (U + \sqrt{U^2 + 4\delta}), \\ r_s &= (-U + \sqrt{U^2 + 4\beta}). \end{aligned} \quad (44)$$

A solution for the pressure P given by solving eq. (40) is $P_0(Y) = -\Lambda(C_0(Y) - C_0(0))$ and the front velocity is then

$$U = \Lambda(C_0(0) - \delta) \cdot r_s + \Gamma_1 C_0(0). \quad (45)$$

For arbitrary values of the physical parameters, this relation gives an implicit equation for U and must be solved numerically. Only in the case where $\delta = 0$, one can find an explicit solution with

$$U = \frac{(\Lambda - \beta)\sqrt{4\Lambda + (\Gamma_1 - \Gamma_2)^2} + (\beta + \Lambda)(\Gamma_1 - \Gamma_2)}{2\Lambda}, \quad (46)$$

showing that contrary to viscous fingering or dendritic growth, the velocity of the steady front is fixed by the complete set of equations and boundary conditions. Moreover a necessary condition for advancing front is that the chemotactic effect must overcome the diffusion inside the cellular domain but also the depletion of nutrients due to mitosis represented by Γ_2 . Mitosis plays the role of a motor (proliferation represented by Γ_1) but is also a brake since it consumes nutrients. To study the 3D effect of diffusion, let us make an expansion for small values of δ when $\Gamma_1 = \Gamma_2 = 0$ for simplification. We get

$$U = U_0 - \frac{(\Lambda + \beta)}{2\Lambda^{3/2}} \left(\Lambda - \frac{\beta}{U_0^2} \right) \delta + O(\delta^2), \quad \text{with } \Gamma_1 = \Gamma_2 = 0, \quad (47)$$

indicating a decrease of the eigenvalue U with a transverse flux, for U_0 not too small. Moreover one must keep in mind the decrease of the length scale of our problem l_0 with decreasing α and δ , so the decrease of the unit

for velocities. The true physical velocities depend on both variations. For very weak velocity, much smaller than $\sqrt{\beta}$ and $\sqrt{\delta}$, one gets

$$U = \Lambda \sqrt{\frac{\delta}{\beta} \frac{1-\delta}{\sqrt{\beta} + \sqrt{\delta}}} \text{ and } U \ll \sqrt{\beta} \text{ or } U \ll \sqrt{\delta}. \quad (48)$$

If $\delta = 0$ we refer to eq. (45).

4.2 Stability of planar steady front

4.2.1 General perturbation analysis in 2D and 3D

The steady front can be observed experimentally only if it is stable. If it is unstable the dispersion relation gives us some insight on possible nonlinear patterns as reported in [4]. Let us study first the case without mitosis at the border. So we imagine a small perturbation of the front $\delta\Omega$ given by $\zeta = \epsilon_2 e^{ikx} e^{\Omega t}$ inducing a perturbation of order ϵ_2 for the pressure and concentration fields as follows:

$$\begin{aligned} P(x, Y, t) &= P_0(Y) + \epsilon_2 \cdot p_{\pm}(Y) e^{\Omega t} \cos(kx), \\ C(x, Y, t) &= C_0(Y) + \epsilon_2 \cdot c_{\pm}(Y) e^{\Omega t} \cos(kx), \end{aligned} \quad (49)$$

where $P_0(Y), C_0(Y)$ are the solutions calculated above eq. (45). Due to the weakness of ϵ_2 , our system of equations, once linearized, can be solved and a calculation tedious but without difficulty gives the dispersion relation Ω as a function of the wave number k . First, the diffusion equation in the moving front gives for $Y > 0$

$$c_{\pm}(Y) = \begin{cases} c_+ e^{-(r_+ \cdot Y/2)}, & \text{if } Y > 0, \\ c_- e^{(r_- \cdot Y/(2\beta))}, & \text{if } Y \leq 0, \end{cases}$$

with

$$r_{\pm} = \begin{cases} r_+ = U + \sqrt{U^2 + 4(\delta + \Omega + k^2)} \\ r_- = -U + \sqrt{U^2 + 4\beta(1 + \Omega + \beta k^2)} \end{cases}$$

and

$$c_-(0) = -\frac{r_+(1-\beta) + r_s + \beta r_l U}{r_- + r_+} \frac{U}{\Lambda}, \quad (50)$$

while the pressure p_- reads

$$p_- = -\Lambda c_-(Y) + (\sigma k^2 + U + \Lambda c_-(0)) e^{kY}, \quad (51)$$

given automatically the dispersion relation

$$\Omega = -(\sigma k^2 + U)k + \frac{U r_s}{2\beta} + \Lambda c_-(0)(r_-(2\beta) - k), \quad (52)$$

if $\Gamma_1 = \Gamma_2 = 0$. Ω is a function of r_+ , r_- and c_- , themselves function of Ω . So eq. (52) is an implicit equation for Ω which must be solved numerically. However, we cannot predict the characteristic of the eigenvalue spectrum. In particular, the existence and unicity of solutions are not assured without numerical investigation.

4.2.2 Results for 2D diffusion

First, we present the numerical results obtained for Ω as a function of k in true 2D diffusion. According to eq. (4.2.1) and eq. (52), Ω is a function of k given in an implicit way. As a consequence, the number of Ω -eigenvalues is not obvious to guess *a priori* and we focus on real and positive values of Ω . Asymptotic analysis is doable for $k \rightarrow 0$ and for k infinite. Near $k = 0$, one can show that a Goldstone mode $\Omega = 0$ for $k = 0$ exists and the limit k close to zero is crucial for global stability of the front. For this limit we get

$$\Omega \sim \frac{\beta}{2\Lambda^{3/2}} \left[\frac{\Lambda + \beta}{U} - \Lambda U \right] k^2 \text{ for } k \rightarrow 0, \quad (53)$$

which proves that the process is unstable for small velocities and recovers stability at “large” velocities given by

$$\Lambda \geq \Lambda_c, \text{ with } \Lambda_c = 1/2(1 + 2\beta + \sqrt{1 + 8\beta}). \quad (54)$$

Above this value for Λ the planar front is stable since Ω is a decreasing function of k . Below Λ_c or for small values of U , whatever the value of β the existence of a domain of unstable modes is usually the signal of strong instability suggesting dendritic patterns [4–6]. For $k \rightarrow \infty$, Ω has an imaginary part but a real dominant part given by $-\sigma k^3$. Intermediate values are reached numerically and solutions are displayed in figs. 4, 5, 6 where we vary one parameter among (Λ, β, σ) , the others remaining fixed. The spectrum is always the same showing a dendritic dispersion relation: strong instability at long wavelengths, stabilization by surface tension. Surface tension defines a cut-off that means a length scale l_c above which patterns are unstable. As an example, radial patterns can be obtained if the radius of the colony is smaller than the cutoff given by

$$l_c \sim 2\pi \frac{\sigma \Lambda^{3/2} U}{\beta(\Lambda + \beta)} \sim 2\pi \frac{\sigma \Lambda(\Lambda - \beta)}{(\Lambda + \beta)\beta}. \quad (55)$$

4.2.3 Results for diffusion in 3 dimensions

When we take into account the 3D effects of diffusion via a transverse flux, there is an increase of the velocities for small U_0 values which is responsible of an increase of the instability behavior as shown in fig. 7. However stability is recovered for large values of δ that is 0.8, being 1 the limiting value.

The fact that an experiment is done in a Petri dish does not suppress the diffusive instability as shown by fig. 7 which is compared to the purely 2D case (with $\delta = 0$). The transverse flux may give an astonishing strength to the instability for a weak value of its amplitude δ . In fact due to the various independent parameters of our model, the variation is not always monotonous and cannot be simply predicted.

The dispersion diagrams established here suggest that in an infinite geometry destabilization of the front gives

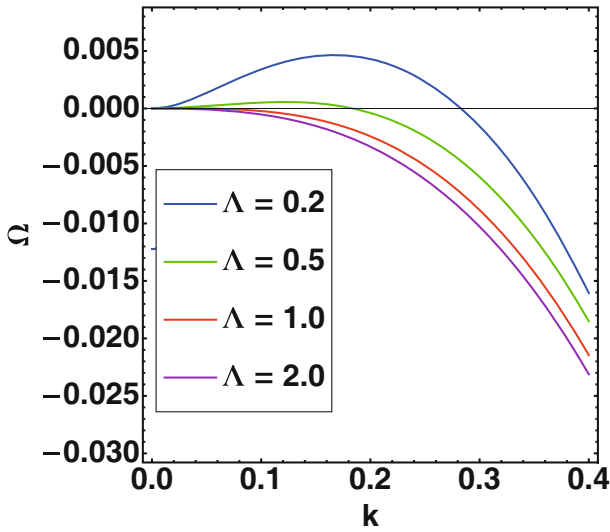


Fig. 4. Dispersion diagram $\Omega(k)$ as a function of the wave number k for different values of the mobility coefficient Λ , according to eq. (52). Simulations are performed with $\delta = 0$, $\beta = 0.1$ and $\sigma = 0.5$. Notice that the value $\Lambda = 1$ is below $\Lambda_c \sim 1.27$ corresponding to a unstable planar front but $\Lambda = 2$ is above Λ_c values and the planar front is then stable.

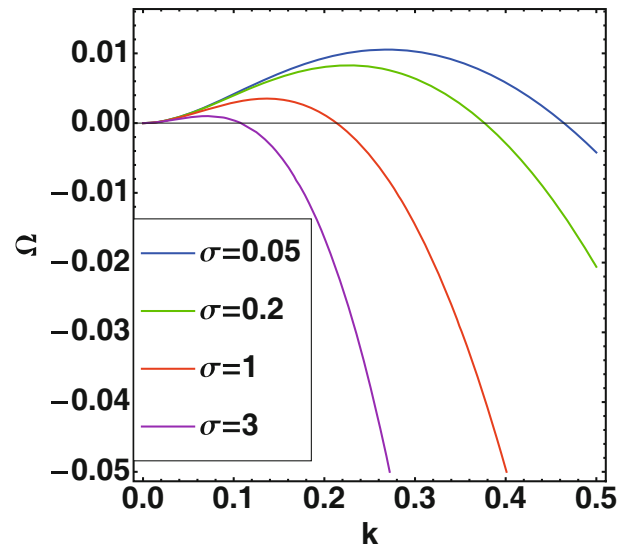


Fig. 6. Dispersion diagram $\Omega(k)$ as a function of the wave number k for different values of the surface tension σ according to eq. (52). Simulations are performed with $\delta = 0$, $\Lambda = 1$ and $\beta = 0.5$.

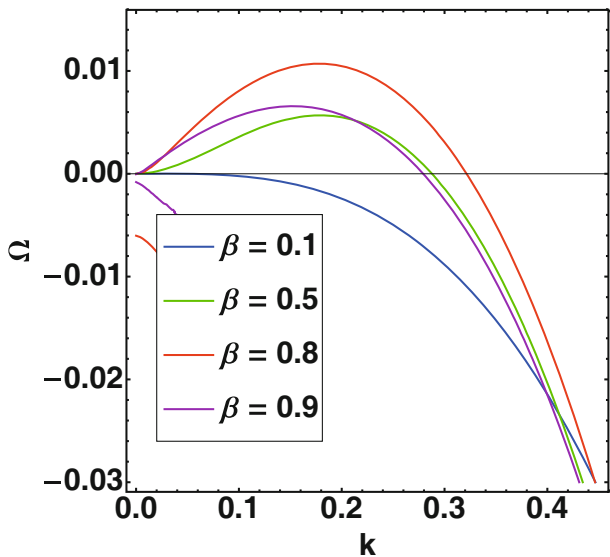


Fig. 5. Dispersion diagram $\Omega(k)$ as a function of the wave number k for different values of the ratio β between the diffusion coefficient in the colonies and in water, according to eq. (52). Simulations are performed with $\delta = 0$, $\Lambda = 1$ and $\sigma = 0.5$. A secondary branch with $\Omega < 0$ exists for $\beta = 0.8$, it has no physical significance.

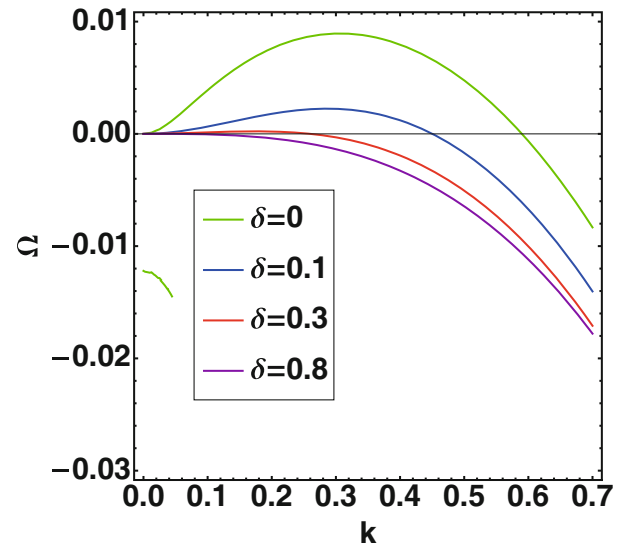


Fig. 7. Dispersion diagram $\Omega(k)$ as a function of the wave number k for different values of δ , measure of the transverse flux according to eq. (52). Simulations are performed with $\Lambda = 0.2$, $\beta = 0.1$ and $\sigma = 0.05$. A secondary branch exists for $\delta = 0$.

patterns which can have infinite amplitude such as in viscous fingering or crystal growth [4–6]: there exists a continuum of unstable wavelengths in the vicinity of $k = 0$. Dendritic patterns are observed for sparsely distributed bacteria solutions [3] but are more questionable for epithelia grown on substrate [16,25]. For epithelia, the ratio between the diffusion coefficient in the tissue and in the liquid β is probably weak and there exists a transverse flux

represented by δ in eqs. (44), (45). However, the saturation of the solution via the transverse flux that maintains a source of nutrients everywhere is not always sufficient to suppress the 2D diffusive instability, imposed by the migration of the colony. One can argue that perhaps we are in the regime where the 2D process is stable having $\Lambda > \Lambda_c$ (54). Clearly the instability of the model imposed by the behavior at $k = 0$ is robust. In the next section, we examine other physical possibilities which may be at the origin of the relative stability of epithelia.

4.3 Compact colonies and the sharp interface model

In the previous example, we conclude that at long times, diffusion will give dendritic patterns, a prediction compatible with bacteria colonies but not with growth of epithelium. Epithelia growing on substrate are more compact, even when they exhibit instabilities. Contrary to physical intuition, these fully nonlinear instabilities are not suppressed by 3D diffusion as we have seen previously. In this paragraph, we want to investigate the modification to limit the strength of the instability. Our scope is to define the conditions for observation of these compact patterns with perhaps weak instabilities as observed in *in vitro* wound healing experiments. To do so the behavior of the dispersion relation $\Omega(k)$ near $k = 0$ is crucial, at large k , the capillary effect behaving as k^3 will saturate the instability and will allow a control of the size of the instabilities. But the small- k behavior is an indicator of a possible threshold for growth instability.

First of all we want to examine the possibility to have a stable front so to avoid a Goldstone mode in this front problem. To simplify, we restrict to 2D diffusion but we examine the possibility to have a nonlinear diffusion equation for the nutrients in the colony. Indeed nonlinearities in the diffusion equation may have 3 origins: nonlinearities of the diffusion coefficient as a function of nutrient concentration or of the concentration gradient, nonlinearities that can arise from the chemotactic model with a more complex mobility law but also from the process of absorption of nutrients. In biochemistry enzymatic transformations lead to the Michaelis-Menten law [21] very commonly used in studies on bacteria colonies [22]. Then the nutrient concentration in the cellular phase $N(Y)$ (to avoid confusion with the linear case, we change the notation from C_s to N) is solution of a complicated nonlinear equation, while in water we keep our ordinary linear law of diffusion. There is little chance to find the analytic solution of $N(Y)$. We simply assume that it exists and that the requirement of a finite value at $N(Y)$ at $-\infty$ selects a unique solution. Rewriting more formally the dispersion relation $\Omega(k)$ (52) than before, we obtain

$$\Omega(k) = -k(\sigma k^2 + \Lambda(N'_0 + n_0)) + \Lambda(N''_0 + n'_0) + \Gamma_1(N'_0 + n_0), \quad (56)$$

where the index 0 means that all the values have to be taken for $Y = 0$, prime and double prime mean first and second derivatives with respect to Y , N and n (the first-order perturbation) being the concentration of nutrients inside the colony. Without specifying the nonlinearity, one can show that if

$$\mathcal{L}(N, \nabla N, \Delta N) = 0, \quad (57)$$

then n is solution of

$$\frac{\partial \mathcal{L}}{\partial N} n + \frac{\partial \mathcal{L}}{\partial \nabla N} \nabla n + \frac{\partial \mathcal{L}}{\partial \Delta N} \Delta n = \Omega n, \quad (58)$$

where we assume $N, \nabla N, \Delta N$ independent in this variation formalism. n satisfies a linear equation and accepts as a solution $\nu_0 N'(Y)$ for $\Omega = 0$ up to a correction in k^2 ,

ν_0 being an arbitrary constant of proportionality. Let us write now the boundary conditions at the front $Y = 0$. Continuity of nutrients and continuity of the flux give at zero order

$$N_0 = C(0) = C_l + 1 \quad \text{and} \quad \beta N'_0 + \Gamma_2 N_0 = -UC_l. \quad (59)$$

The zero order prescribes the logarithmic derivative of the nonlinear solution at the front. At next order we derive

$$\begin{aligned} N'_0 + n_0 &= -UC_l + c_+ \\ \beta(N''_0 + n'_0) + \Gamma_2(N'_0 + n_0) &= U^2 C_l - r_+ c_+ / 2. \end{aligned} \quad (60)$$

If Ω and k vanish, $r_+ = 2U$. Then knowing that $n' = \nu_0 N'$, we get $\nu_0 = -1$ except for very specific values of our problem so irrelevant. This value of ν_0 means $\Omega = 0$ and nonlinearities cannot suppress the Goldstone mode. However, more attention has to be paid on the behavior near $k = 0$. If Ω decreases negatively with k^2 we get a possibility for observation of a quasi-steady front. If mitosis is included, the limit U small is singular but looking for finite values of U we get

$$\Omega = \frac{\beta}{2\Lambda} \left(\frac{\Lambda + \beta}{\Lambda - \beta} - (\Lambda - \beta) \right) k^2, \quad (61)$$

which gives the same answer as eq. (53), which corresponds to the linear case. Again the front is expected to be highly unstable at low velocities. The effect of nonlinearities which have been extensively studied in mathematics at the origin of all the variants on the Keller-Segel model [17] are perhaps more surprising. Analytical predictions are really difficult to get: for example for the Michaelis-Menten law [21], we can prove only the existence of the Goldstone mode. But we cannot do more without knowing the base solution N_0 , which results from the solution of a nonlinear ordinary differential equation (O.D.E.). Recent works [32, 33] are concerned by exact derivation of this kind of (O.D.E.) called Fisher-like equation but we are not aware of a solution for the Michaelis-Menten law. We do not consider the case of nonlinear diffusion but the case of nonlinear mobility for the chemoattractants is more easy to handle. Nonlinear mobility has been introduced because cells do not measure only the gradient of N but they can be sensitive to more complex functions. For the chemotaxis, the model is extended to $\mathbf{V} = \nabla \chi(N)$ the only restriction being $\Lambda(N) = \chi'(N)$ positive for chemoattractants. In this case, focussing directly on the behavior for $k = 0$ we get

$$\Omega = \Lambda(N_0)(N''_0 + n'_0) + \frac{A_1(N_0)}{\Lambda(N_0)} n_0(0)U, \quad (62)$$

A_1 being the first derivative of Λ with respect to N . U is given by a nonlinear equation

$$U = \frac{\Lambda(N_0) - \beta}{\sqrt{\Lambda(N_0)}} \quad \text{with} \quad N_0 = 2U / (U + \sqrt{4\beta + U^2}). \quad (63)$$

One can show that if Λ is a slightly increasing function of N so that $A_1/\Lambda \ll 1$, then we get $\Omega(0) = -\frac{A_1}{2\Lambda^3} (\Lambda^2 - \beta^2)$

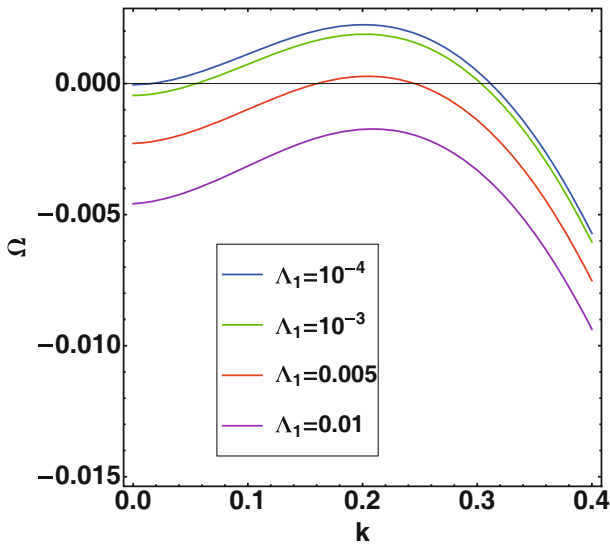


Fig. 8. Dispersion diagram $\Omega(k)$ as a function of the wave number k for different values of the mobility coefficient Λ_1 given by eq. (62). Simulations are performed with $\Lambda = 1, \beta = 0.3$ and $\sigma = 0.1$.

so for $k = 0$, Ω is negative and a planar stable front can be observed. This calculation is explicit only if Ω is weak (see also fig. 8). However for arbitrary values the spectrum may be more complex as shown by fig. 9 which exhibits domains where Ω has an imaginary part. Considering fig. 8, for specific values of the parameters, varying Λ_1 , it is possible to observe planar fronts (purple curve in fig. 8) and also a stable, steady periodic pattern with a prescribed wavelength corresponding to the vicinity of the red curve in fig. 8. One can argue that the nonlinearity which is introduced to stabilize the front is “unphysical” since it has a tendency to increase the linear behavior and usually nonlinearities are responsible of saturation. However bacteria use chemotaxis as natural self-engineering adaptation [11], especially at low nutrient concentration and such behavior is typical of small nutrient concentration.

5 Discussion

Recent published experimental papers on migration and growth of an epithelium [16, 12, 34, 35] do not mention the possibility of chemotaxis as a possible driving force. So we use the published data simply to check that it may be a possible scenario. Let us give an evaluation of the dimensionless parameters entering into the model. We refer to eq. (42) which makes the link between dimensionless parameters and physical quantities. Values of the parameter Λ , motor of our migration process both for the case of epithelium or bacteria are difficult to find. We discuss first an epithelium made of MDCK cells experiments [12, 34]. Taking into account the fact that the average velocity of MDCK cells on solid substrate is $40 \mu\text{m}$ per hour [12], this value is consistent with our velocity unit estimated to be $\sqrt{D_l/(\tau_c(1+\alpha))}$. Indeed according

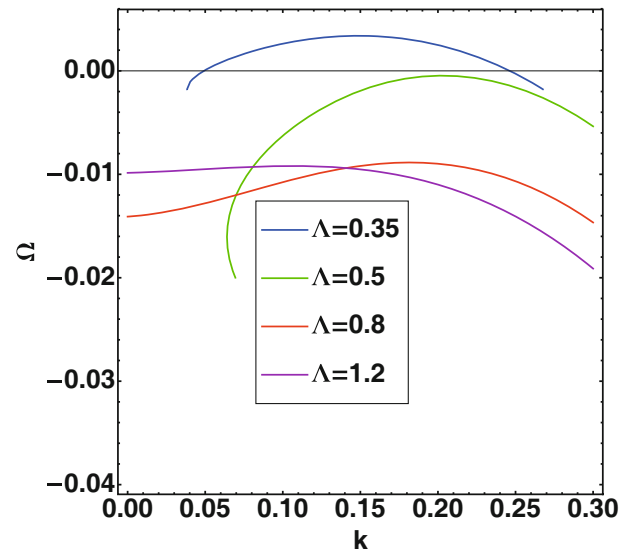


Fig. 9. Dispersion diagram $\Omega(k)$ as a function of the wave number k for different values of Λ . Simulations are performed with $\Lambda_1 = 0.025, \beta = 0.3$, and $\sigma = 0.5$.

to [1] the uptake time is of order half an hour, D_l in water is $10^{-10} \text{m}^2/\text{s}$ (that we decrease to take into account α) so our effective $D_l \sim 10^{-11} \text{m}^2/\text{s}$ which gives approximately $0.7 \mu\text{m}/\text{s}$ so $260 \mu\text{m}$ per hour. The dimensionless velocity $U = (\Lambda - \beta)/\sqrt{\Lambda}$ (eq. (46)) is then $U \sim 40/260 \sim 0.15$. β being the ratio between the diffusivity in the tissue and the water is about $\beta = 1/100$, then we deduce that $\Lambda \sim 0.04$ giving a typical wavelength for instability of order 16σ in dimensionless units. Let us evaluate now the dimensionless capillary number. In [34], the tension at the border of a MDCK epithelium is estimated to be $\tilde{\sigma} \sim 0.07 \text{nN}\mu\text{m}^{-1}$ while the friction on a rigid substrate is about $\zeta = 1 \text{nN s}/(\mu\text{m})^3$ which allows to determine the permeability $K = l_0/\zeta$. K being given by $\sqrt{D_l\tau_c}/\zeta = 1.410^5$, SI finally gives $\sigma \sim 3.510^{-3}$. Knowing that the length unit is $140 \mu\text{m}$ we get the typical length scale for the instability about $8 \mu\text{m}$ which is the cell size for this particular experiment [12]. This is coherent with experimental observations but at the limit of validity of the model.

In a different experiment involving a migrating cell sheet of Madin-Darby canine kidney, Treppe *et al.* [35] also observe an undulation of the advancing front with a wavelength of order $100 \mu\text{m}$. They measure the forces and conclude that there is a traction force perpendicular to the front, a result consistent with our pressure model $P = -\Lambda(C_s - C_{sf})$, C_{sf} being the front concentration. Estimating the pressure in physical units, we get $P \sim \Lambda D_l \zeta / l_0$ which gives the correct order of magnitude that is 1000Pa . Moreover the stress grows quite exponentially with the distance from the front also in agreement with our model.

For bacterial colonies, our model may give a new way to explain the quasi-exponential behavior of the mass transfer due to chemotaxy according to eq. (44). Indeed experimental results aiming to measure $\hat{\Lambda}$ are not obtained

directly but based on a model for the concentration. When mitosis is subdominant, our prediction for the length decay of chemoattractant concentration is $\sqrt{\Lambda}/(\Lambda-1)\sqrt{D_I\tau_c}$, our Λ being itself related to its physical value by eq. (42). It varies linearly with the bacterium and the chemoattractant densities. In other experimental geometry, the model for regular fronts can be adapted without difficulty [36].

6 Conclusion

We have established an analytical model for studying the stability properties of a class of coupled P.D.E. governing front evolution due to chemotaxis. Our formulation based on the mixture model where the interface is diffuse is suitable for numerical investigation of living colonies moving in a chemoattractant field. We consider only chemoattractants which are not a by-product of the colony itself and which are consumed by the cells of the colony. Our model allows to derive the correct boundary conditions when the front between the colony and the environment is abrupt. Then the migration of the colony is transformed into a free-boundary problem which can be addressed analytically in simple geometries. Here we have investigated planar fronts and their stability which gives some insights on the nonlinear behavior of the front. Chemotaxis is known to be essentially an unstable process which is confirmed here when the chemotaxis attraction is weak. Surprisingly, when it increases, the stability of diffusion occurs as for dendritic growth and the front recovers stability. Also surface tension stabilizes short wavelength perturbations fixing a capillary length, the limit of stability of circular patterns. We investigate also other possible stabilization processes. These effects are physically relevant as the saturation of the solution in chemoattractants or a strong but localized mitosis at the front.

However, if we are successful in explaining the dendritic patterns for sparsely distributed bacteria (having $\beta \sim 1$) deriving a dispersion relation typical of dendritic growth [4], perhaps the relative compactness of epithelia as observed in [12, 16] may involve more complex interactions. We examine also the possibilities of nonlinearities of the chemotaxis process concerning the law of attraction and the uptake. Our conclusion concerning the Michaelis-Menten law for the uptake, in the absence of known exact solutions for the planar front is that the Goldstone mode is maintained and probably this nonlinearity is not enough. More success concerns nonlinearity in the chemoattraction itself which does not affect the diffusion equation and the boundary conditions. Here we can show that typical mobility laws give stable fronts or weakly unstable fronts. The main conclusion however is that if we want to interpret epithelia or *a priori* biofilms [37], elastic effects must be introduced which is possible in the mixture model framework [23] as it has been done for tumor growth. Ultimately, the comprehension of the shape instability and the pattern formation in multiphase models is of utmost importance for a wide range of problems relating to tissue growth, remodeling and morphogenesis under chemotaxis.

This work was supported in part by ‘‘AAP Physique Cancer 2012’’. We would like to thank Pascal Silberzan for sending an unpublished figure of epithelium growing on a substrate. We are very indebted to Pasquale Ciarletta and Julien Dervaux for helpful discussions.

Open Access This is an open access article distributed under the terms of the Creative Commons Attribution License (<http://creativecommons.org/licenses/by/3.0>), which permits unrestricted use, distribution, and reproduction in any medium, provided the original work is properly cited.

References

1. K.W. Rogers, A.F. Schier, *Annu. Rev. Cell Dev. Biol.* **27**, 377 (2011).
2. V. Sourjik, J.P. Armitage, *EMBO j.* **29**, 2724 (2010).
3. E. Ben-Jacob, H. Shmueli, O. Shochet, A. Tenenbaum, *Physica A* **187**, 378 (1992).
4. J.S. Langer, *Rev. Mod. Phys.* **52**, 1 (1980).
5. M. Ben Amar, *Journ. Phys. I* **3**, 353 (1993).
6. M. Ben Amar, E. Brener, *Phys. Rev. Lett.* **71**, 589 (1993).
7. Y. Couder, *Growth patterns: from stable curved fronts to fractal structures*, in *Chaos, Order and Patterns*, edited by R. Artuso, P. Cvitanovic, G. Casati (Plenum Press, 1991).
8. M. Ben Amar, *Phys. Rev. A* **44**, 3673 (1991).
9. F. Argoul, E. Freysz, A. Kuhn, C. Lger, L. Potin, *Phys. Rev. E* **53**, 1777 (1996).
10. F. Argoul, E. Freysz, A. Kuhn, C. Lger, L. Potin, *Phys. Rev. A* **44**, 3673 (1991).
11. E. Ben-Jacob, H. Levine, *J. R. Soc. Interface* **3**, 197 (2006).
12. M. Reffay, L. Petitjean, S. Coscoy, E. Grasland-Mongrain, F. Amblard, A. Buguin, P. Silberzan, *Biophys. J.* **100**, 2566 (2011).
13. J.R. King, S.J. Franks, *Mathematical Modeling of Biological Systems*, Vol. 1, edited by A. Deutsch, L. Bruschi, H.M. Byrne, G. Vries, H. Herzel (Birkhauser, 2007) p. 175.
14. J.S. Lowengrub *et al.*, *Nonlinearity* **23**, R1 (2010).
15. M. Eisenbach, ‘‘Bacterial Chemotaxis’’ *Encyclopedia of life Sciences* (Nature Publishing Group, 2001) pp. 1-14.
16. A. Puliafito, L. Hufnagel, P. Neveu, S. Streichan, A. Sigal, D.K. Fygenson, B.I. Shraiman, *Proc. Nat. Acad. Sci. U.S.A.* **109**, 739 (2012).
17. E.F. Keller, L.A. Segel, *J. Theor. Biol.* **26**, 399 (1970).
18. L. Corrias, B. Perthame, H. Zaag, *Milan J. Math.* **72**, 1 (2004).
19. J. Dolbeault, B. Perthame, *C. R. Math. Acad. Sci. Paris* **339**, 611 (2004).
20. M.A. Herrero, J. Velazquez, *Journ. Math. Biol.* **35**, 177 (1996).
21. L. Menten, M.I. Michaelis, *Biochem. Z.* **49**, 333 (1913).
22. J.B. Xavier, E. Martinez-Garcia, K.R. Foster, *Amer. Naturalist* **174**, 1 (2009).
23. P. Ciarletta, L. Foret, M. Ben Amar, *J. R. Soc. Interface* **9**, 305 (2011).
24. A. Saez, E. Anon, M. Ghibaudo, M.O. du Roure, J.-M. Di Meglio, P. Hersen, P. Silberzan, A. Buguin, B. Ladoux, *J. Phys.: Condens. Matter* **22**, 19 (2010).

25. S. Mark, R. Shlomovitz, N. Gov, S. Nir, M. Poujade, E. Grasland-Mongrain, P. Silberzan, *Biophys. J.* **98**, 361 (2010).
26. M. Doi, A. Onuki, *J. Phys. II* **2**, 1631 (1992).
27. G. Caginalp, P. Fife, *Phys. Rev. B* **33**, 7792 (1986).
28. G. Caginalp, *Arch. Rach. Mech. Anal.* **92**, 205 (1986).
29. J.W. Cahn, J.E. Hilliard, *J. Chem. Phys.* **28**, 258 (1958).
30. J.W. Cahn, J.E. Taylor, *Acta Metall.* **42**, 1045 (1994).
31. M. Ben Amar, *Phys. Fluids A* **4**, 2641 (1992).
32. N. Kudryashov, *Phys. Lett. A* **342**, 99 (2005).
33. M. Hayek, *Appl. Math. Comput.* **218**, 2407 (2011).
34. O. Cochet-Escartin, *Dynamique de fermeture de blessures circulaires modèles: aspects expérimentaux et théoriques*, PhD thesis of University Pierre et Marie Curie, Paris (Avril 2013).
35. X. Trepât, Mi.R. Wasserman¹, T.E. Angelini, E. Millet, D.A. Weitz, J.P. Butler, Jeffrey J. Fredberg, *Nat. Phys.* **5**, 426 (2009).
36. X. Wang, T. Long, R.M. Ford, *Biotech. Bioengin.* **109**, 1622 (2012).
37. J. Dervaux, J.C. Magniez, A. Libchaber, *Growth and form of Bacillus subtilis biofilms*, preprint (2012).